RSC Advances

ROYAL SOCIETY OF CHEMISTRY

www.rsc.org/advances

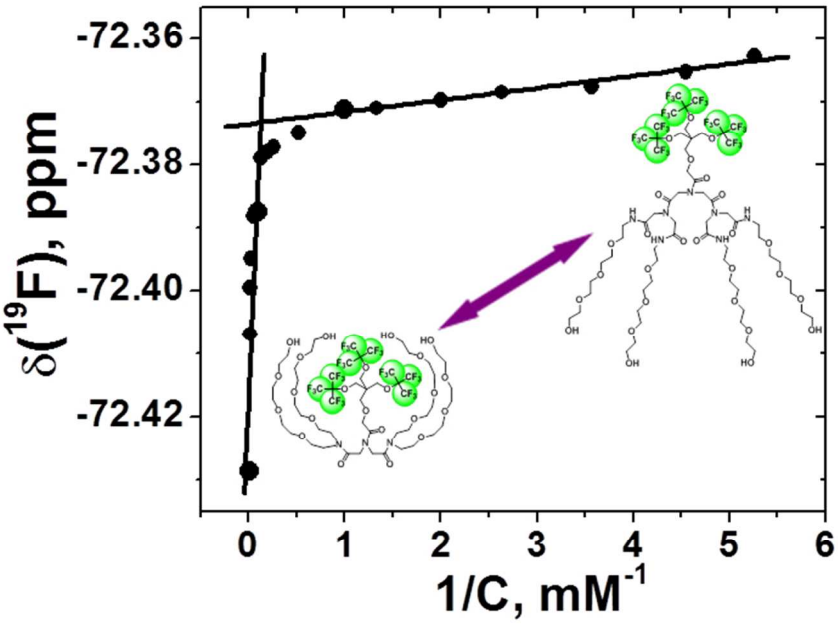

Graphical Abstract
69x49mm (300 x 300 DPI)

Conformational transition of a non-associative fluorinated amphiphile in aqueous solution†

Marc B. Taraban,[1‡] Li Yu,[2‡] Yue Feng,[1] Elena V. Jouravleva,[3] Mikhail A. Anisimov,[3,4] Zhong-Xing Jiang,[2] Y. Bruce Yu[1*]

[1]Department of Pharmaceutical Sciences, University of Maryland, Baltimore, MD 21201, USA
[2]School of Pharmaceutical Sciences, Wuhan University, Wuhan, Hubei 430071, China
[3]Institute for Physical Science and Technology, University of Maryland, College Park, MD 20742, USA
[4]Department of Chemical and Biomolecular Engineering, University of Maryland, College Park, MD 20742, USA

*Corresponding author: Department of Pharmaceutical Sciences, 20 Penn Street, Baltimore, MD 21201, USA; Email: byu@rx.umaryland.edu; Phone: 410-706-7514; Fax 410-706-5017.
‡Marc B. Taraban and Li Yu contributed equally to this work.

†Electronic Supplementary Information (ESI) available: Experimental procedures, ^{1}H, ^{13}C and ^{19}F NMR spectra of the intermediate compounds of the FIT-27 synthesis, and their MS and elemental analysis data. HPLC and MS data of final product, SAXS structure factor information, and comparison and differential of pair-wise distance distribution functions of FIT-27 at different concentrations. See DOI: 10.1039/b000000x/

Abstract

Amphiphiles comprise a hydrophobic moiety and a hydrophilic moiety. A common property of many amphiphiles is self-associate in aqueous solutions, driven by the need to shield the hydrophobic moiety from water. This feature has been utilized extensively to create various nano-scale architectures from amphiphiles. However, to effectively control amphiphile behavior, one should have the ability to both promote and prevent self-association. Fluorinated amphiphiles are especially prone to self-association, thus presenting a big challenge in developing non-associative amphiphiles. In this work, we solve this challenge by creating steric hindrance to association. The resulting fluorinated asymmetric amphiphile remains monomeric well above its apparent critical micelle concentration and up to its solubility limit, as demonstrated by small-angle X-ray and neutron scattering, dynamic light scattering and NMR diffusometry techniques. Not being able to associate intermolecularly, the amphiphile undergoes an intramolecular conformational transition, akin to protein folding, to wrap its hydrophilic moiety around its hydrophobic fluorocarbon moiety to shield it from water. This work demonstrates that steric hindrance is an effective tool in creating non-associative amphiphiles.

Introduction

Amphiphilic molecules with covalently linked hydrophobic and hydrophilic moieties have wide applications in chemistry, material science, medicine, and beyond.[1] Their most remarkable property—the propensity to self-association in aqueous solutions, driven by the need to shield the hydrophobic moiety from water—is considered an intrinsic property of amphiphiles. Indeed, the associative property of amphiphiles has been exploited to great extent to create various nanoscale architectures.[2] In a challenging quest for various novel nano-scale assemblies of different shapes—spheres, disks, cones, cylinders, fibers, etc.—of great importance is the nature of their "building bricks."[3] Recent outburst in the development of novel synthetic approaches afforded many new amphiphilic macromolecules with different shapes, branching algorithm and degree, generation levels, and functional groups at the core and the periphery.[4,5,6] What is missing from current research effort is how to prevent amphiphile association in aqueous solutions. This is important because effective control of amphiphile behavior requires the ability to both promote and prevent their association. Here, we report a non-associative fluorinated amphiphile which remains monomeric well above its apparent critical micelle concentration (CMC). Prevention of self-association is based on steric hindrance, which is realized in the form of an asymmetric amphiphile comprised of a hydrophobic core and a hydrophilic dendron.

Generally, in supramolecular chemistry of amphiphilic molecules, one could distinguish *intermolecular* assembly—the aggregation of a number of such molecules into certain nano-scale construct; or *intramolecular* assembly—the reorganization of a single molecule into the most thermodynamically stable structure. Intermolecular assembly is more easily experimentally detected and, hence, extensively studied and better understood[5] as opposed to intramolecular assembly, which is often an intermediate step in inter-molecular assembly.[7] A notable example of standalone intramolecular assembly is the transition of charged polyamidoamine (PAMAM) dendrimers, which change their conformations in response to changes in solution pH and ionic strength.[8] Such intramolecular assembly is attributed to the effects of counterions, which prevent intermolecular assembly.[9]

Both inter- and intramolecular assembly of amphiphiles are driven by a plethora of non-covalent forces, including, but not limited to, electrostatic interactions, hydrophobic interactions, hydrogen bonding, donor-acceptor interactions, and van der Waals forces, *etc*. For instance, a number of building units have been synthesized capable to self-assemble into three-dimensional supramolecular constructs[5]

driven, *e.g.,* by hydrogen bonding,[10] or by electrostatic interactions triggered in the presence of transition or rare earth metal ions.[11] Of course, whether an amphiphile will undergo intermolecular association or intramolecular conformational transition will critically depend on its structure. Understandably, intermolecular assembly is also regulated by the shape of the building unit, since steric hindrances often control the assembly process. Indeed, the overwhelming majority of building units have conic or truncated conic shapes with the assembly triggering function located at the 'tip' ('top') of the cone. Such shape minimizes the hindrances when the above units are organized first into spheres (or disks), then into cylinders, which in turn can further pack into cubic lattices.[5] Conical shape of the single unit also facilitates the preparation of the so-called dendronized linear polymers where a number of dendrimers are attached to numerous binding sites along the polymeric backbone.[12] The structural organization of the dendronized polymers affords even wider variety of nano-assembled shapes—toroids, nanoribbons, nanotubes, *etc*.[5]

Amphiphilic dendrimers,[13] which comprise a hydrophobic core and a hydrophilic dendron, are some of the most versatile building units for nano-scale structures due their strong tendency to self-associate.[3] However, such structural organization might also provide an excellent structural motif for non-associate amphiphiles for two reasons. On the one hand, their bi-conical shape may create steric hindrance to intermolecular association in water. On the other hand, amphiphiles with hydrophilic dendrons have the potential to undergo intramolecular conformational transitions. For example, amphiphiles made of hydrophobic aromatic dendrons covalently linked to hydrophilic poly(ethylene glycol) (PEG) chains switch conformation in response to change of solvent polarity. In nonpolar solvents such as THF, the hydrophilic PEG chains are tightly packed and shielded from the apolar solvent by the hydrophobic moiety; but in polar solvents such as MeOH, the hydrophilic PEG chains become extended and wrap around the hydrophobic dendrons to shield them from the polar solvent.[14] Although these previously observed conformational changes in organic solvents were in response to changes in solvent polarity, they nonetheless suggest the possibility that one part of an amphiphile could be covered by another part, thereby providing an alternative to intermolecular association.

Compared with hydrocarbons, which are hydrophobic but lipophilic, fluorocarbons are hydrophobic and lipophobic at the same time. Consequently, fluorocarbons tend to form their own phase, the so-called fluorous phase.[15] As a result, fluorinated amphiphiles typically are more prone to intermolecular association as opposed to their non-fluorinated counterparts. For example, sodium perfluorooctanoate (a linear perfluorinated amphiphile) has a critical micellar concentration (CMC) of *ca*. 30 mM,[16] while its

non-fluorinated analog, sodium octanoate, has a CMC of ~ 400 mM.[17] From this viewpoint, it is particularly challenging to develop a fluorinated amphiphile that does not self-associate in aqueous solutions. In this paper, we describe the synthesis of a non-associative fluorinated amphiphile with 27 equivalent fluorine atoms, FIT-27 (Figure 1), as well as its structural characterization in aqueous solutions in a wide concentration range. Structurally, this asymmetric fluorinated amphiphile is comprised of a hydrophobic fluorocarbon core and a hydrophilic hydrogenous dendron as the solubility enhancer in aqueous media.

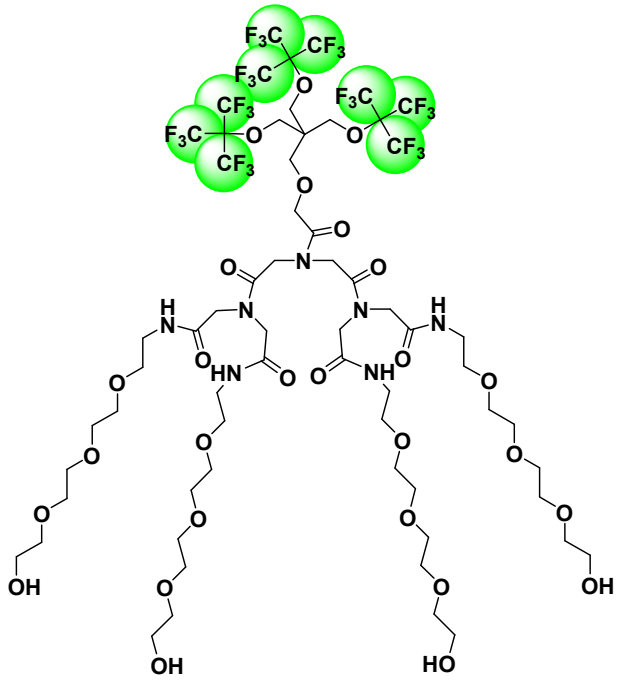

Figure 1. Structural formula of the fluorinated amphiphile FIT-27 with 27 equivalent fluorine atoms.

Here, we demonstrate that instead of self-association, this fluorinated amphiphile undergoes a conformational transition in which the hydrophilic chains wrap around the hydrophobic dendron to shield it from water. In ^{19}F NMR, such conformational transition manifests itself very similar to micellization with a characteristic critical concentration. Therefore, to reveal such intramolecular changes, we investigated the solution structure of amphiphilic dendrimer using a combination of small-angle X-ray and neutron scattering (SAXS/SANS), dynamic light scattering (DLS), and NMR diffusometry.

Results and Discussion

Potential micellization of FIT-27 in buffered aqueous solutions could be most conveniently monitored by ^{19}F NMR. First, it has long been known that ^{19}F chemical shifts are far more sensitive towards changes in molecular environment than ^{1}H chemical shifts.[18] Second, all fluorine atoms in FIT-27 molecule are magnetically equivalent, therefore a sharp (~0.02 ppm peak width) singlet is observed in all ^{19}F NMR spectra (see **Figure 2** and ESI†). This significantly simplifies the monitoring of ^{19}F chemical shift ($\delta(^{19}F)$) changes, presumably reflecting concentration-dependent association or conformational transition of FIT-27 (**Figure 2** (A)).

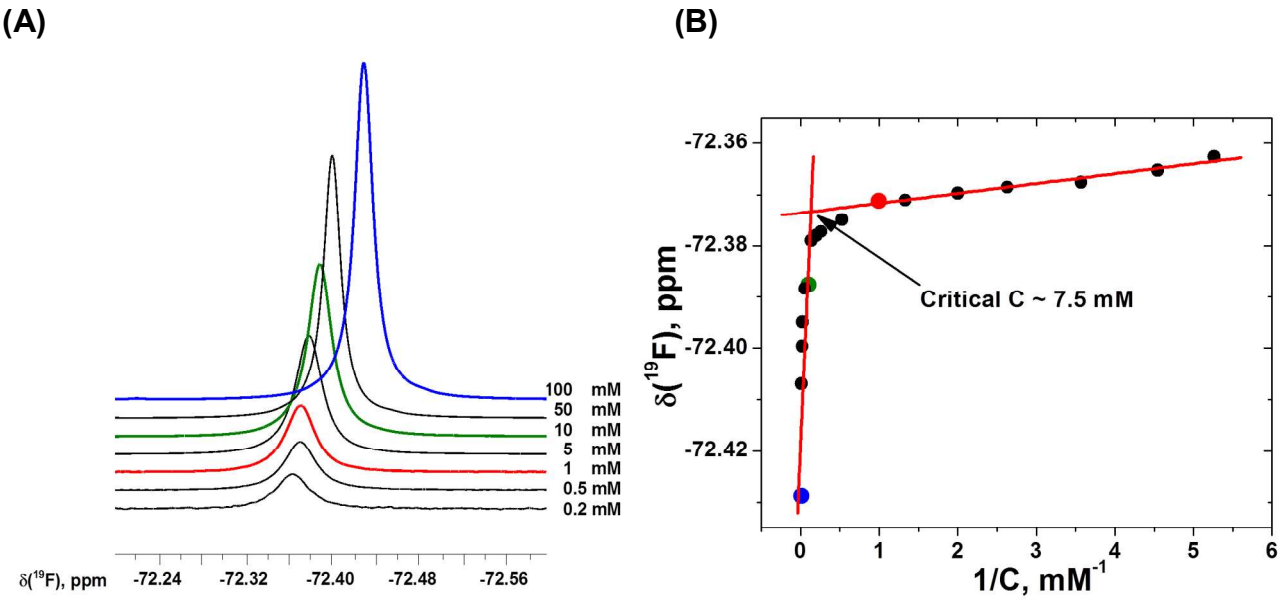

Figure 2. (A) ^{19}F spectra of FIT-27 in PBS (pH 7.4) at different concentrations. $\delta(^{19}F)$ ppm values are given with TFA as the external standard (-76.55 ppm). Signal intensities are rescaled for better visibility. Red, green, and blue traces show 1, 10, and 100 mM, respectively. (B) Critical concentration of FIT-27 determined from the $\delta(^{19}F)$ vs. $1/C$ plot. Red, green, and blue circles correspond to 1, 10 and 100 mM, respectively.

To explore the possibility of micellization by FIT-27, we used a well-established approach based on the dependence of $\delta(^{19}F)$ vs. the concentration reciprocal, $1/C$.[19] It is expected that below the CMC, $\delta(^{19}F)$ will remain essentially unchanged since the amphiphiles should exist predominantly as non-associated monomers. Above the CMC, significant upfield shift in $\delta(^{19}F)$ is expected as a result of

micelle formation, which transfers the fluorocarbon moiety from an aqueous to a fluorous environment. Thus, the plot of $\delta(^{19}F)$ vs. $1/C$ should yield two straight lines intersecting at 1/CMC. Indeed, as seen from **Figure 2**(B), the $\delta(^{19}F)$ vs. $1/C$ plot of FIT-27 resulted in the expected pattern with the intersection point of two straight lines corresponding to a CMC of ~7.5 mM.

The results presented in Figure 2(B) on FIT-27 are entirely consistent with those from its two close analogs, which also display an intersection around 7-8 mM in the $\delta(^{19}F)$ vs. $1/C$ plot.[20] Further, such behaviors are consistent with micelle formation, as observed in other fluorinated amphiphiles, where micellization leads to a high-field shift of the ^{19}F chemical shift.[16] Hence one might conclude that FIT-27 forms micelles with CMC of ~ 7.5 mM. However, the absolute changes of $\delta(^{19}F)$ in **Figure 2**(B) amounts only to ~ 0.05 ppm in the concentration range from 0.2 mM to 100 mM, which is much smaller than the ^{19}F chemical shift change observed in the micellization of other fluorinated amphiphiles, which is ~ 2 ppm.[19] This raises the question as to what kind of micelles had formed by FIT-27, or even, whether micelles had formed at all. To find out, we used scattering and diffusometry techniques, including SAXS SANS, DLS and PFG NMR to directly observe FIT-27 at three concentrations: 1 mM (well below CMC), 10 mM (slightly above CMC), and 100 mM (well above CMC).

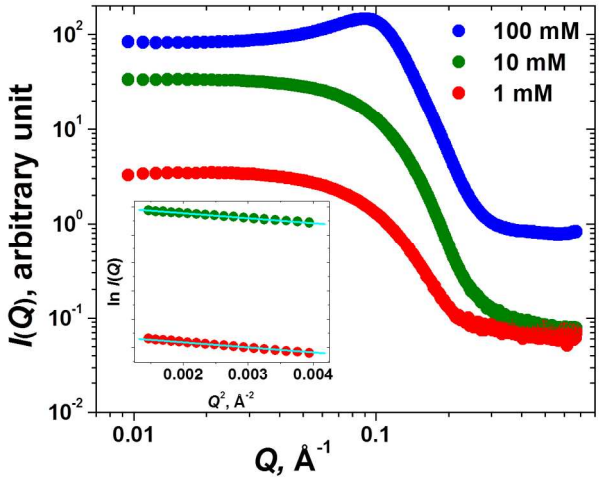

Figure 3. SAXS scattering profiles of FIT-27 in PBS buffer (pH 7.4) at different concentrations. Inset shows the linearity of the Guinier plot for globular particles, *ln I*(*Q*) vs. Q^2. Red: 1mM FIT-27; green: 10 mM FIT-27; blue: 100 mM FIT-27.

As seen from the SAXS scattering profiles of $I(Q)$ vs. Q (**Figure 3**), FIT-27 solutions at the three concentrations show no evidence of the aggregation at low Q, which is flat. In contrast, aggregation would have caused an uptick in the low Q range (below 0.03 $Å^{-1}$).[21] Moreover, the Guinier plots for globular particles, $ln\ I(Q)$ vs. Q^2,[22] are perfectly linear for both 1 mM and 10 mM FIT-27 solutions (inset in **Figure 3**), which strongly suggest the absence of aggregation and the monodispersity of scattering particles at 1 mM and 10 mM. No Guinier analysis of 100 mM data could be performed due to strong structure factor peak centered around 0.1 $Å^{-1}$ (**Figure 3**).

Indirect Fourier transformation of the scattering data for 1 mM and 10 mM FIT-27 solutions result in the corresponding pair-wise distance distribution functions, $P(r)$, shown in **Figure 4** (A) & (B). From $P(r)$, the low resolution structure of the scattering particles can be constructed, as shown in Figure 4 (C) and (D). As seen from Figure 4, solution structures of FIT-27 are different at 1 mM and 10 mM (see also the differential of corresponding $P(r)$ functions in the ESI†, Figure S20).

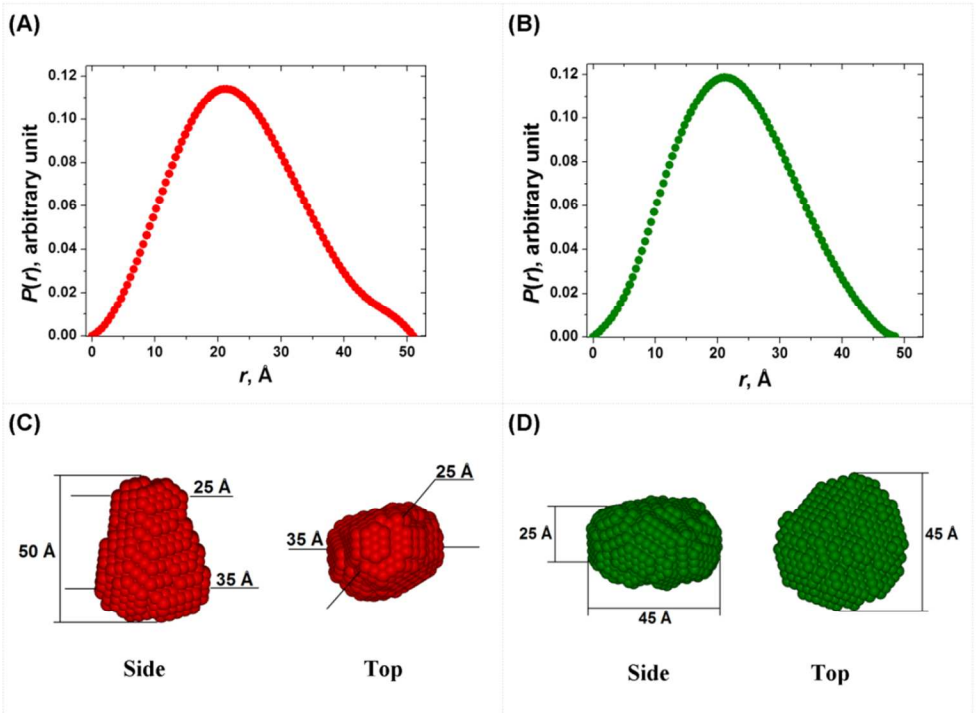

Figure 4. Pair-wise distance distribution function $P(r)$ (A, B) and corresponding *ab initio* restored low resolution 3D shapes (C, D) of FIT-27 in PBS buffer (pH 7.4). (A) 1 mM FIT-27, d_{max} ~ 51 Å, R_g = 17.8 Å; (B) 10 mM FIT-27, d_{max} ~ 47 Å, R_g = 17.2 Å; (C) side and top views of FIT-27 dendrimer 3D shape at 1 mM concentration; (D) side and top views of FIT-27 dendrimer 3D shape at 10 mM concentration. Red: 1mM FIT-27; green: 10 mM FIT-27. $P(r)$ functions are normalized to account for the difference in FIT-27 concentration.

At 1 mM, FIT-27 has an elongated drop-like shape, with maximum dimension d_{max} ~ 51 Å, and radius of gyration R_g = 17.8 Å (**Figure 4** (A) and (C)). Based on the FIT-27 chemical structure, one might suggest that the top smaller portion of the drop-like shape (~ 25 Å in diameter) belongs to the fluorocarbon moiety, while the bulkier bottom portion (~ 35 Å in diameter) is formed by the four more flexible and longer ethylene oxide chains (**Figure 4** (C)). When the concentration of FIT-27 increases to 10 mM, the conformation of the molecule changes, which is also consistent with critical point of the chemical shift δ(^{19}F) change in **Figure 2**(B). At 10 mM, FIT-27 in solution acquires the shape of an oblate spheroid with maximum dimension d_{max} ~ 47 Å, and radius of gyration R_g = 17.2 Å (**Figure 4** (B) and (D)). Both d_{max} and R_g suggest that the structure of FIT-27 at 10 mM is more compact than at 1 mM.

The SAXS scattering profile of FIT-27 at 100 mM also shows no signs of large assemblies—the scattering profile at 100 mM is essentially flat in the range of $Q < 0.03$ Å^{-1} (Figure 3). On the other hand, at 100 mM, an apparent peak, which is absent at 1 and 10 mM, is observed around $Q \sim 0.1$ Å^{-1} (Figure 3). Similar peaks are commonly attributed to interparticle interaction due to certain order of their organization,[8] and their appearance at high concentrations is attributed to the intermolecular structure factor.[23] In general, SAXS scattering intensity could be expressed as $I(Q) \sim P(Q) \times S(Q)$, where $P(Q)$ is the form factor of the scattering particles, and $S(Q)$ is the structure factor; in dilute solutions, $S(Q) = 1$.[24] Here, the form factor $P(Q)$ characterizes the shape of the individual scattering particle, while in non-dilute systems, the structure factor $S(Q)$ reflects the interference due to the dense packing of the scattering particles when the distance between particles becomes of the same order of magnitude as the size of a particle itself.

Since no aggregation of FIT-27 is observed at 100 mM, one can assume that the form factor $P(Q)$ at 100 mM could be approximated by normalizing the scattering profile of FIT-27 at 10 mM, *i.e.*,

$$P(Q, 100\text{ mM}) \cong \quad 10 \times P(Q, 10\text{ mM}) = 10 \times I(Q, 10\text{ mM}) \qquad (1)$$

The absence of the aggregates at 10 mM as well as perfect linearity of Guinier plot (Figure 3, inset) suggests that at this concentration of FIT-27 the interparticle interference could be negligible, *i.e.*, $S(Q, \textit{10}\text{ mM}) \cong 1$. Subsequent division of the scattering data for 100 mM FIT-27 by such normalized values for 10 mM solution will give the desired structure factor $S(Q)$ at 100 mM (Figure 5, i.e.,

$$S(Q,100\,\text{mM}) = \frac{I(Q,\,100\,\text{mM})}{P(Q,\,100\,\text{mM})} = \frac{I(Q,\,100\,\text{mM})}{10 \times I(Q,\,10\,\text{mM})} \quad (2)$$

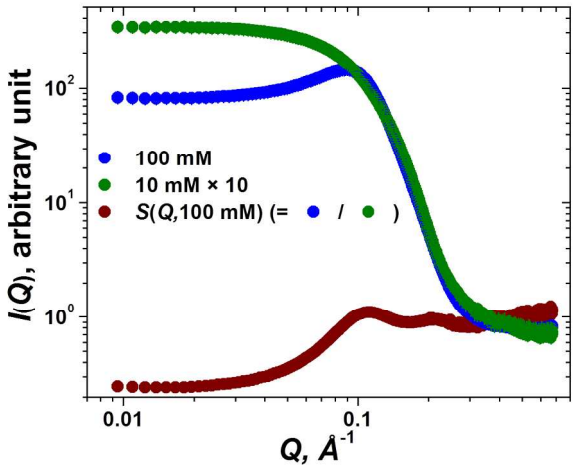

Figure 5. Structure factor $S(Q)$ contributing to the broad peak observed in SAXS scattering profiles of 100 mM FIT-27 solution. Green: 10 mM FIT-27 multiplied by 10 to model the form factor $P(Q)$; blue: 100 mM FIT-27; brown: structure factor $S(Q,100\text{ mM})$ obtained by dividing the blue trace by the green one.

This $S(Q)$ vs. Q profile could be instructive to select proper structure factor when modeling size distribution, volume fraction, and the shape of the scattering particles with certain order of organization in non-dilute solutions. Since the $S(Q)$ vs. Q in Figure 5 is very similar to the theoretical description of the structure factor for hard spheres in non-dilute solutions (see Figure S21, ESI†), we modeled the experimental $I(Q)$ vs. Q profile for 100 mM FIT-27 solution using the corresponding *IRENA* 2.46[25] routine based on the structure factor for hard spheres from the NIST SAS software.[26] The results of the modelling show that low resolution shape of the scattering particle is close to the one suggested at 10 mM within the range of ±3 Å (see Figure S22 and description, ESI†). In general, one might get an approximate estimate of the average distance d between the scattering particles in 100 mM solution based on the position of structure factor peak Q_s (~ 0.091 Å^{-1}, Figure 3) using standard Bragg's law:[22]

$$d = 2\pi/Q_s, \qquad d \sim 70\ \text{Å} \quad (3)$$

To get more clear insight with respect to the location of the fluorocarbon moiety in the above low-resolution structure of FIT-27, we have opted to perform SANS experiments on 1 mM, 10 mM, and 100

mM FIT-27 solutions in H_2O-based PBS (pH 7.4)—same as in SAXS experiments. There are numerous experimental evidences suggesting that due to the big difference between coherent neutron scattering length densities (SLD) of fluorinated and hydrogenous moieties of a molecule,[27] one might try to selectively visualize the fluorinated part in H_2O without D_2O additions. Indeed, *e.g.*, for linear C_8F_{17}-nonioic amphiphiles, neutron SLD for the hydrophobic (fluorinated) part is more than 7 times higher as compared to the hydrophilic (hydrogenous) part (cf. 4.3×10^{10} cm^{-2} vs. 0.6×10^{10} cm^{-2}).[28] Therefore, we attempted to reconstruct the low-resolution 3D shapes of FIT-27 from SANS scattering profiles in expectation that partial contrast matching in H_2O will allow us to visualize the fluorinated groups, i.e., water will at least partially mask the hydrogenous moiety due to their closer SLDs (-0.56×10^{10} cm^{-2} for water vs. 0.6×10^{10} cm^{-2} for hydrogenous part) with no such effect on the fluorinated part due to their very different SLD (-0.56×10^{10} cm^{-2} for water vs. for 4.3×10^{10} cm^{-2} for fluorocarbons).[28]

Unlike SAXS data, due to the strong background signal from H_2O, SANS profile of FIT-27 at 1 mM is very noisy (Figure 6 (A)). Fortunately, at 10 mM, scattering from FIT-27 is much stronger than the background. Indirect Fourier transform of $I(Q)$ of 10 mM resulted in $P(r)$ function (Figure 6 (B)) with dimensional parameters very close to those observed for the same solution in SAXS experiment— d_{max} ~ 48 Å, R_g = 17.3 Å. Reconstructed low-resolution 3D shape of FIT-27 in 10 mM solution from SANS data also appears to be very similar to the oblate spheroid reconstructed from SAXS data (cf. dark green shapes for results from SAXS and light green shapes for results from SANS, Figure 6 (C)). However, in SANS experiments, partial contrast matching between the buffer and the hydrogenous moiety of FIT-27 has allowed us to mask a portion of the hydrogenous moiety—this resulted in a Saturn-like shape with a visualized central fluorinated core (light green shapes in Figure 6 (C)). This Saturn-like shape is also consistent with the observed shoulder peak in $P(r)$ at r ~ 35 Å (Figure 6 (B)), which corresponds to the size of the fluorinated core (Figure 6 (C)).

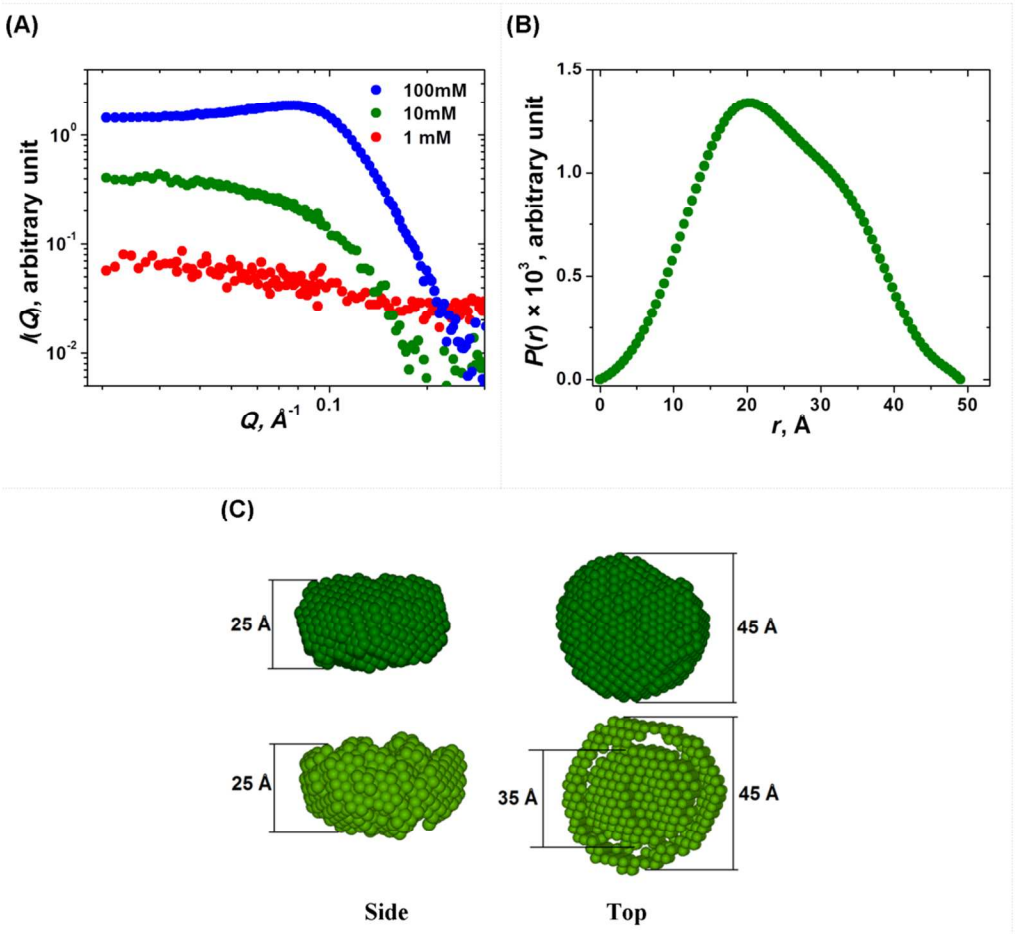

Figure 6. (A) SANS scattering profiles of FIT-27 in PBS buffer (pH 7.4) at different concentrations. Red: 1mM FIT-27; green: 10 mM FIT-27; blue: 100 mM FIT-27. (B) Pair-wise distance distribution function $P(r)$ derived from the SANS scattering data of the 10 mM FIT-27 solution. $d_{max} \sim 48$ Å, $R_g = 17.3$ Å. (C) Comparison of *ab initio* restored low resolution 3D shapes of FIT-27 dendrimer at 10 mM in PBS; green (top): side and top views of FIT-27 dendrimer 3D shape of oblate spheroid from SAXS data; light green (bottom): side and top views of FIT-27 dendrimer 3D Saturn-like shape from SANS data.

Based on the SAXS and SANS results, we conclude that the abrupt change of the ^{19}F chemical shift at the critical concentration is not the result of micellization. Rather, it is the result of a transition between an extended conformation and a compact conformation of FIT-27. Below the critical concentration, FIT-27 adopts an extended drop-shaped conformation with the fluorocarbon moiety exposed to water; above CMC, FIT-27 adopts a compact conformation with the PEG chains wrapping around the fluorocarbon moiety to shield it from water, as illustrated **Figure 7**.

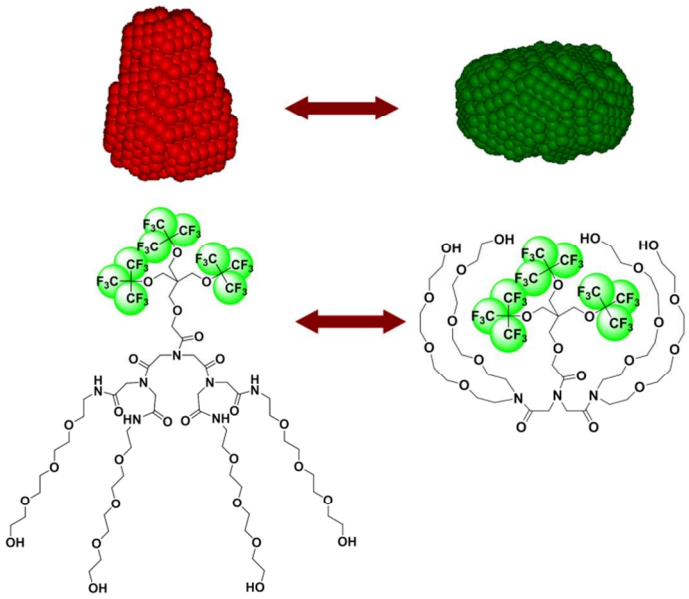

Figure 7. Conformational transition of FIT-27 as its concentration increases from 1 mM (red) to 10 mM (green). Transitions are shown for low resolution 3D shapes restored from SAXS data (top) and pictorial presentations of the FIT-27 molecule in extended and compact forms (bottom).

Note that PEG chains are much more polar than fluorocarbons. This explains the very small change of the ^{19}F chemical shift displayed by FIT-27 during this process. In essence, intra-molecular conformation transition transfers the fluorocarbons from an aqueous to a PEG environment while inter-molecular micellization would have transferred the fluorocarbons from an aqueous to a fluorous environment. The former causes much smaller change in environment polarity that the latter, and thereby much smaller ^{19}F chemical shift change.

Like associative amphiphiles prone to intermolecular association, this fluorinated amphiphile has its hydrophobic group exposed to water below its critical concentration. Above the critical concentration, this non-associative fluorinated amphiphile covers its hydrophobic group through intramolecular conformational transition rather than through intermolecular association, as in the associative amphiphiles. Such concentration-induced conformational transition bears certain similarity to crowding-induced compaction and folding of polypeptide chains/proteins.[29] One possible driving force of such transformation could be the solubilization energy of the hydrophobic fluorocarbon moiety of FIT-27 by water molecules. Below the critical concentration (~ 7.5 mM), the free energy of solubilization of the fluorocarbon moiety of FIT-27 is probably low enough, and the molecule favors

drop-like conformation of high conformational entropy with extended hydrophilic tails. As the concentration of FIT-27 reaches the critical point and beyond, the crowding effect drives up the free energy of solubilizing the fluorocarbon moiety by water. This leads to conformational transition to more beneficial shape where the hydrophobic moiety is shielded from water molecules. Micellization/association was not observed presumably due to the unfavorable sterical hindrances created by the bulky shape of the fluorocarbon moiety.

The absence of large FIT-27 assemblies was also confirmed in DLS experiments. As seen from **Figure 8**(A), for all three concentrations (1, 10, and 100 mM), three very close values of the decay times of the autocorrelation functions in FIT-27 solutions were observed: τ (1 mM) = 32 μs; τ (10 mM) = 37 μs; τ (100 mM) = 37 μs. From these correlation times the collective diffusion coefficient D_c of FIT-27 can be obtained, which is 8.3×10^{-11}, 7.2×10^{-11} and 7.1×10^{-11} m^2/s at 1, 10 and 100 mM, respectively. From D_c, the average hydrodynamic radius R_h of hydrated FIT-27 molecules can be calculated using the Stokes-Einstein equation, which is 31, 33 and 34 Å, respectively at 1, 10 and 100 mM.

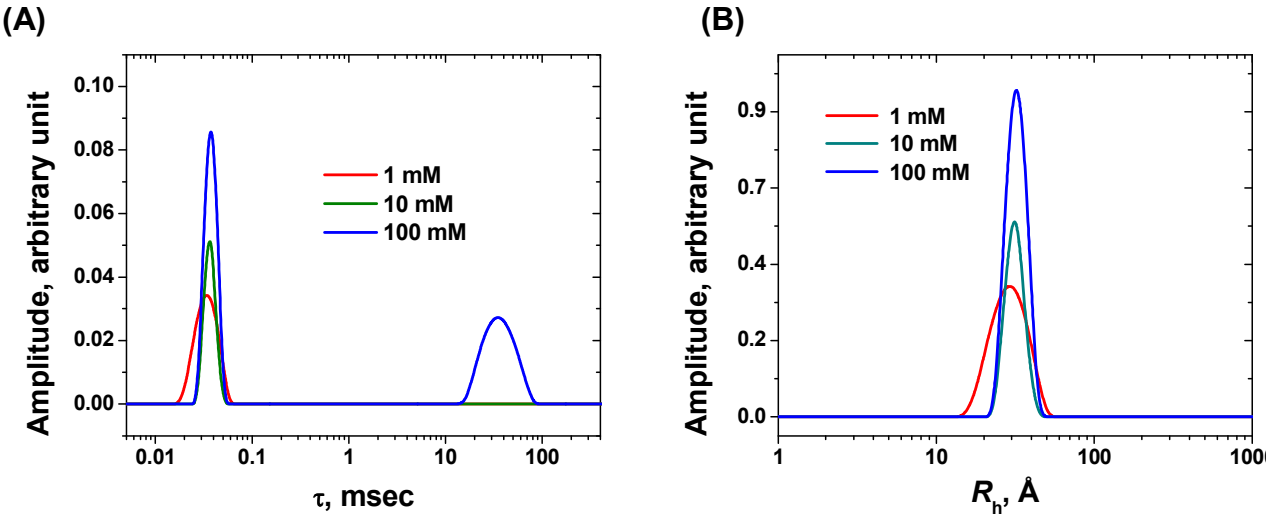

Figure 8. (A) Distribution of the decay time of the autocorrelation functions in FIT-27 solutions from DLS experiments: τ (1 mM) = 32 μs; τ (10 mM) = 37 μs; τ (100 mM) = 37 μs and 40 ms. (B) Size distribution of scatterers in FIT-27 solutions from DLS experiments. Hydrodynamic radii of the monomer FIT-27: R_h (1 mM) = 31 Å; R_h (10 mM) = 33 Å; R_h (100 mM) = 34 Å. Red: 1 mM, green: 10 mM, blue: 100 mM.

Figure 8(B) shows the distribution of R_h at these three concentrations. The width of the distribution in 10 and 100 mM solutions is very close to each other (cf. green and blue traces, **Figure 8**(B)), consistent with the similar oblate spheroid shapes of the molecule reconstructed from SAXS data (**Figure 4**(D)).

The noticeably broader R_h distribution of FIT-27 in 1 mM solution (red trace, **Figure 8**(B)) could be due to the observed in SAXS more asymmetrical drop-like shape of FIT-27 with extended ethylene oxide chains. The observed peaks of the hydrodynamic radii (Figure 8(B)) could be attributed to non-aggregated FIT-27 monomers, and are in a good agreement with the dimensional parameters of FIT-27 molecule concluded on the basis of SAXS and SANS data. Since the radius of gyration R_g from SAXS/SANS is the averaged distance of all scattering elements from the center of gravity of the scattering particle weighted by the scattering contrasts, while the hydrodynamic radius R_h from DLS reflects the radius of the hydrated particle and is derived from diffusion measurements, R_g is usually smaller than R_h. For example, for solid spheres, theory gives $R_g/R_h \sim 0.7\text{-}0.8$.[30] It has been shown that, for compact dendrimers, $R_g/R_h \sim 0.5\text{-}0.7$,[31] which is consistent with our observations in the present paper (*e.g.*, for 1 mM FIT-27 solution, $R_g/R_h \sim 0.57$).

The distribution of the decay times of the autocorrelation function at 100 mM also shows a peak with very slow relaxation times $\tau \sim 40$ ms (**Figure 8**(A)). Such along relaxation times could not be ascribed to the Brownian diffusion motions of particles. Rather, this peak reflects the average times of collective motion of organized densely packed FIT-27 particles with overlapping hydration layers at 100 mM in the laser spot. Indeed, such slow motions are consistent with the very slow dynamics of FIT-27 at 100 mM—in a full agreement with the SAXS data (Figure S22, ESI†), which favor the very dense packing of the FIT-27 particles restricting the faster motion of the particles.

Effects of dense packing and the absence of large assemblies in FIT-27 solutions were also confirmed by the measurements of the self-diffusion coefficient D_s using the PFG NMR technique through the ^{19}F signal from FIT-27. To account for any concentration-driven viscosity effects, the FIT-27 self-diffusion coefficient D_s(FIT-27) is normalized by the water self-diffusion coefficient $D_s(H_2O)$ measured in the same solution through the $^{1}H_2O$ signal. **Figure 9**(A) shows the concentration dependence of normalized D_s(FIT-27)/$D_s(H_2O)$ values as well as the values of individual diffusion coefficients (Table inset, **Figure 9**(A)).

As seen from Figure 9(A), no significant changes in the self-diffusion of FIT-27 molecules were detected when its concentration increased from 1 mM to 10 mM. This observation corroborates the absence of large aggregates of FIT-27 as well as the negligible intermolecular interference at 10 mM, even though this is already above the critical concentration of 7.5 mM. At 100 mM, noticeable retardation of FIT-27 diffusion is observed, and this is in full agreement with the slow motion of non-

associated but densely packed FIT-27 molecules with overlapping hydration layers concluded on the basis of SAXS and DLS data for this concentration.

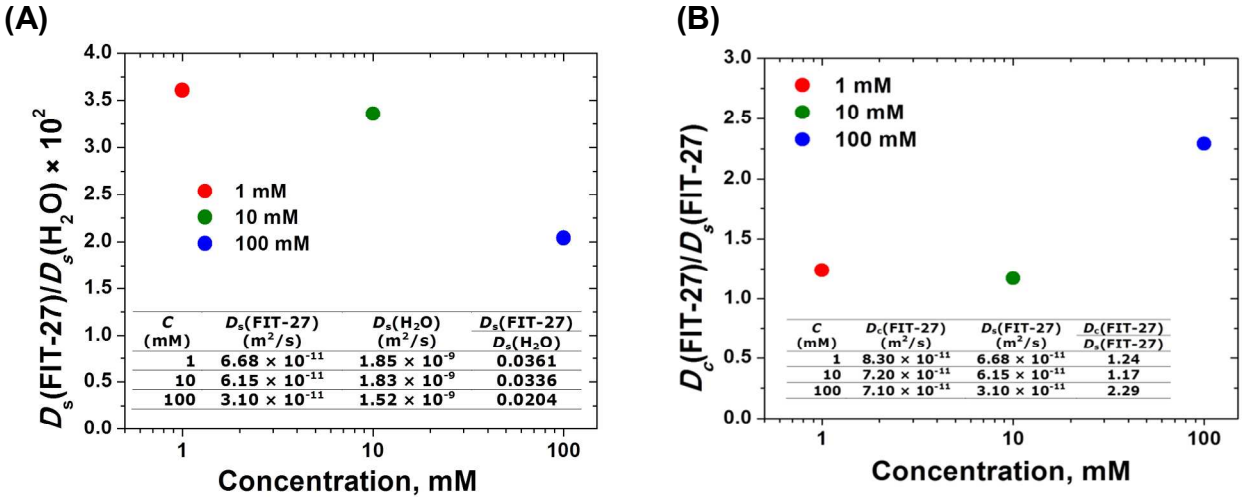

C (mM)	D_s(FIT-27) (m^2/s)	D_s(H$_2$O) (m^2/s)	D_s(FIT-27) / D_s(H$_2$O)
1	6.68 × 10^{-11}	1.85 × 10^{-9}	0.0361
10	6.15 × 10^{-11}	1.83 × 10^{-9}	0.0336
100	3.10 × 10^{-11}	1.52 × 10^{-9}	0.0204

C (mM)	D_c(FIT-27) (m^2/s)	D_s(FIT-27) (m^2/s)	D_c(FIT-27) / D_s(FIT-27)
1	8.30 × 10^{-11}	6.68 × 10^{-11}	1.24
10	7.20 × 10^{-11}	6.15 × 10^{-11}	1.17
100	7.10 × 10^{-11}	3.10 × 10^{-11}	2.29

Figure 9. (A) Normalized self-diffusion coefficient of FIT-27 at 1, 10 and 100 mM. Inset shows the table with individual values of the self-diffusion coefficients of FIT-27, D_s(FIT-27), and water, D_s(H$_2$O). (B) Ratio of the collective diffusion coefficient D_c of FIT-27 determined by DLS and the self-diffusion coefficient D_s of FIT-27 determined by PFG NMR. Red: 1 mM, green: 10 mM, blue: 100 mM. Inset shows the table with individual values of the collective diffusion coefficient D_c(FIT-27) and the self-diffusion coefficient D_s(FIT-27) at different concentrations.

Of note, the observed collective diffusion coefficient D_c of FIT-27 from DLS measurements is generally larger than the self-diffusion diffusion coefficient D_s from PFG NMR experiments (Figure 9(B)). Such differences can be explained by the analysis of collective vs. self- diffusion coefficients in the framework of frictional formalism for binary solutions.[32] It has been shown that collective (D_c) and self- diffusion (D_s) are described by different relationships depending on the friction coefficients between the components of the binary system:

$$D_c \sim (f_{12} c_1)^{-1} \text{ and } D_s \sim (f_{12} c_1 + f_{22} c_2)^{-1} \quad (4)$$

Here, f_{12} and f_{22} refer to the solvent-solute and solute-solute molar hydrodynamic friction coefficients, respectively; c_1 and c_2 are solvent and solute concentrations, respectively.[32] From Eq. 3, it follows that in non-ideal systems, D_c should be always somewhat greater that D_s. Therefore, the experimentally

observed differences between D_c (from DLS) and D_s (from NMR) evidently result from the interparticle interaction between amphiphilic FIT-27 molecules and their interaction with medium (water). Indeed, it has been demonstrated that in the case of nonpolar particles in nonpolar solutions where such interactions are small, the two diffusion coefficients D_c and D_s are close to each other,[33] as has been exemplified in the case of non-polar polystyrene particles in non-polar toluene.[34] However, if solute particles interact with each other and the solvent, D_c becomes significantly greater than D_s, as it has been demonstrated for reverse AOT micelles in the octane/H_2O mixture.[35] And the stronger is the interparticle interaction (f_{22}), the greater becomes the gap between the above two diffusion coefficients. When the concentration of FIT-27 increases from 1 to 10 mM, the ratio of D_c/D_s remains almost unchanged (~1.2, Figure 9(B))—consistent with similar interparticle interactions at these concentrations. At 100 mM, intermolecular interactions among FIT-27 molecules are presumably larger than at 1 mM and 10 mM due to the short inter-molecular distance and the hydration layer overlap—hence, the gap between D_c and D_s becomes much larger and their ratio grows almost twice (~2.3, Figure 9(B)).

In summary, abrupt change of the NMR chemical shift at certain critical concentration is conventionally used as an indication of micellization of amphiphiles. However, as have been shown by the combination of SAXS, SANS, DLS, and NMR diffusometry measurements, the observed critical point in the concentration dependence of the NMR chemical shift could also reflect the conformational transition of the amphiphile molecule in the absence of any aggregation. One possible driving force of such transformation could be the solubilization energy of the hydrophobic fluorocarbon moiety of FIT-27 by water molecules. At low concentration, like other surfactants, FIT-27 exists in the monomeric state with its hydrophobic fluorocarbon moiety exposed with extended hydrophilic tails. As the concentration increases, again like other surfactants, FIT-27 needs to have its hydrophobic moiety shield from water, presumably due to the unfavorable free energy of solving a large number of hydrophobic groups. However, unlike other surfactants, whose shape permit close packing into, e.g., spherical micelles, the drop-like shape of FIT-27 molecule makes such close packing of bulky fluorine moiety impossible. On the other hand, the hydrophilic chains are long and wide enough to cover the fluorocarbon part. As a result, the hydrophilic chains wrap around the hydrophobic moiety to shield it from water. In the case of dendrimeric amphiphiles, such as FIT-27, micellization in general might be incompatible with the shape of the molecule due to above mentioned reasons. Shielding of the hydrophobic part is achieved through intra-molecular conformational transition, resulting in the

hydrophilic part wrapping around the hydrophobic part, a process that bears some resemblance to protein folding in a crowded environment.

Conclusions

While intermolecular association in aqueous solutions is considered a common feature of amphiphiles, this work demonstrates that it is possible to use steric hindrance to create amphiphiles that remain monomeric in water close to the solubility limit. Without the ability to associate intermolecularly, the amphiphile undergoes an intramolecular conformational transition as the concentration increases, leading to the hydrophilic moiety wrapping around the hydrophobic moiety to shield it from water. This requires the hydrophilic moiety to have sufficient size and flexibility. This requirement, along with the requirement of steric hindrance, is readily implemented in the form of amphiphilic asymmetric dendrimer. This works paves the way to engineer non-associative amphiphiles to suite various applications.

Experimental Section

Synthesis of fluorinated amphiphile FIT-27

Synthesis of FIT-27, which has 27 chemically equivalent fluorine atoms followed earlier described procedure,[20] which was simplified by the introduction of an additional methylene group between the fluorocarbon moiety and the hydrophilic moiety. The synthesis also included the protection/deprotection steps using *tert*-butyl and trityl groups which make their removal much easier as compared to earlier used benzyl protective group. All modifications made compared to the previous version of the synthesis[20] afforded the large scale preparation of the resulting FIT-27 amphiphile (refer to ESI† for detailed description of the synthesis scheme and NMR and MS spectra of the intermediate products).

Sample preparation for physical and structural characterizations

For all characterizations, 100 mM stock solution of FIT-27 was prepared in phosphate-buffered saline (PBS, 50 mM sodium phosphate, 100 mM NaCl, pH 7.4 in H_2O) which prior to dilutions was filtered through a 0.2-μm filter. For ^{19}F chemical shift $\delta(^{19}F)$ measurements, the concentrations of FIT-27 range from 0.2 mM to 100 mM. For all other characterizations, including PFG NMR, SAXS, SANS and DLS, FIT-27 solutions of 1, 10 and 100 mM were prepared.

NMR spectroscopy measurements

All ^{1}H and ^{19}F NMR experiments were carried out using a Varian INOVA 400 NMR spectrometer (Varian, Inc., 399.75 MHz for ^{1}H and 376.11 MHz for ^{19}F) equipped with a broadband detection probe with Z-gradient. ^{19}F NMR chemical shifts in FIT-27 solutions are estimated using trifluoroacetic acid (TFA) as the ^{19}F external standard ($\delta_{TFA}(^{19}F)$ = -76.55 ppm).[36] The self-diffusion coefficient D_s of FIT-27 was measured by the BPP-LED (bipolar pulse longitudinal eddy current delay) method,[37] using the pulsed-field gradient (PFG) NMR technique (refer to ESI† for detailed description of the NMR characterizations and parameters used).

Small-Angle X-Ray Scattering (SAXS) and Small-Angle Neutron Scattering (SANS)

Solution X-ray scattering data were acquired on the BioSAXS-1000 (Rigaku Co.) instrument equipped with confocal Max-Flux optics. Data collection was done using the Pilatus 100K (Dectris, Ltd.) detector positioned 0.48 m from the sample capillary with 8 keV Cu Kα incident radiation from the Micromax-007HF rotating anode source resulting in the observable Q-range of ~ 0.009–0.70 $Å^{-1}$. Scattered radiation was detected, subject to a 7-keV low-energy cutoff. Q-axis mapping was done using scattering from a silver behenate standard sample. Twenty five μL of each FIT-27 solution were pumped into a cylindrical quartz capillary cell using the autosampler of the instrument. SANS data were collected using a 30-m SANS instrument (NG-3) at NIST.[38] Monochromatic neutrons at λ = 6 Å with a wavelength spread ($\Delta\lambda/\lambda$) of 0.14 were detected on a 64 cm × 64 cm two-dimensional detector. The low-Q configuration used neutron focusing lenses and an 8 Å neutron wavelength. Lower monochromaticity of neutrons in SANS as compared to X-rays in SAXS, more accurate Q-axis calibration in SAXS, as well as signficantly larger pixel size of the detector (~ cm range in SANS and ~ μm range in SAXS) could be a reason of slight difference in the structure peak positions, ~ 0.091 $Å^{-1}$ (SAXS) vs ~ 0.089 $Å^{-1}$ (Figure 3 vs Figure 6(A)). For SANS experiments, 400 μL of each solution were aliquoted into a titanium cell with 1-mm path length between two quartz windows used for SANS measurements at the

National Institute of Standards and Technology (NIST) Center for Neutron Research (NCNR). Blank buffer solution scattering collected in the same capillaries (for SAXS) and cells (for SANS) was subtracted from all solution scattering data, respectively.

Solution scattering profiles $I(Q)$ vs. Q used to study the structures of FIT-27 at 1 mM, 10 mM, and 100 mM were processed using the *ATSAS* software (European Molecular Biology Laboratory, Hamburg).[39,40] This software was also used to restore low resolution 3D structures of FIT-27 solutions based on simulated annealing algorithm. The analysis of pair-wise distance distribution functions for globular particles $P(r)$ was performed using the linear regularization method of indirect Fourier-transformation using the program GNOM. $P(r)$ is proportional to the probability of finding different vector lengths connecting two unit-volume elements within the scattering particle, and $P(r) = 0$ happens at the maximum linear dimension of the scattering particle, d_{max} (i.e., for $r \geq d_{max}$, $P(r) = 0$). The radius of gyration of the scattering globular particle, R_g, is derived from the second moment of $P(r)$ using the following equation

$$R_g^2 = \frac{\int_0^{d_{max}} P(r) r^2 dr}{2\int_0^{d_{max}} P(r) dr} \quad (5)$$

where R_g is the root mean square distance of all unit-volume elements from the center of gravity of the scattering particle weighted by the scattering contrasts. *IRENA 2.46* software[25] for *IGOR Pro 6.3* (WaveMetrics, Inc.) was used to analyze the size distribution and structure factor in 100 mM FIT-27 solution. At 100 mM concentration, SAXS and SANS yield very similar scattering profiles (Figure 3 vs Figure 6(A)), but the SANS data have high contribution from H_2O scattering (SANS experiments were done in 100% H_2O). In contrast, SAXS data show excellent signal statistics. Hence the analysis for 100 mM FIT-27 solutions was based on the SAXS data (refer to ESI† for detailed description of the SAXS and SANS experiments and the data processing techniques).

Dynamic Light Scattering (DLS) Experiments

Prior to DLS experiments, all samples were additionally filtered through a 0.2 μm filter. One mL of each sample was aliquoted into cylindrical glass vials (6 mm in diameter). Data collection of 1 mL of each sample in cylyndrical glass vials (6 mm OD) started after complete equilibration at 25 °C (±

0.1 °C) in the cavity of the light scattering setup. The scattering angle in all experiments was 90°. DLS experiments were performed with a PhotoCor Instruments equipment,[41] and the software *DynaLS* (SoftScientific, Inc.) was used to process the scattering data (refer to ESI† for detailed description of the DLS experiments and the data processing techniques).

Acknowledgements

Work at the University of Maryland was supported in part by the National Science Foundation (CBET 1303031) and the National Institutes of Health (EB012003). Dynamic light scattering experiments were conducted at Light Scattering Center, University of Maryland (College Park). Work at Wuhan University was supported by the National Natural Science Foundation of China (No. 21372181). We also thank Dr. J. Ilavsky (Argonne National Lab) for assistance with *IRENA 2.46* software, Dr. A. Grishaev (NIDDK, NIH) for help in conducting SAXS experiments, and Dr. B. Hammouda (NIST, NCNR) for help with SANS experiments. This work has been done in the frames of NIST NCNR Proposal No. S31-50 and is based upon activities supported in part by the National Science Foundation under Agreement No. DMR-0944772.

References

1 J. Israelachvili, *Intermolecular and Surface Forces*; Academic Press: London, 2nd ed., 1992.

2 C. Domb, J. L. Lebowitz, G. Gompper and M. Schick, *Self-Assembling Amphiphilic Systems*; Academic Press: London, 1994.

3 (a) V. Percec, D. A. Wilson, P. Leowanawat, C. J. Wilson, A. D. Hughes, M. S. Kaucher, D. A. Hammer, D. H. Levine, A. J. Kim, F. S. Bates, K. P. Davis, T. P. Lodge, M. L. Klein, R. H. DeVane, E. Aqad, B. M. Rosen, A. O. Argintaru, M. J. Sienkowska, K. Rissanen, S. Nummelin and J. Ropponen, *Science,* 2010, **328**, 1009-1014; (b) X. Li, J. Haley, H. Schlaad, R. Ju, Y. Geng, *Soft Matter,* 2010, **6**, 2037-2043; (c) A. Roy, S. Comesses, M. Grisel, N. Hucher, Z. Souguir and F. Renou, *Biomacromolecules,* 2014, **15**, 1160-1170.

4 S. M. Grayson and J. M. J. Fréchet, *Chem. Rev.,* 2001, **101**, 3819-3867.

5 B. M. Rosen, C. J. Wilson, D. A. Wilson, M. Peterca, M. R. Imam and V. Percec, *Chem. Rev.,* 2009, **109**, 6275-6540.

6 X. Yue, M. B. Taraban, L. L. Hyland and Y. B. Yu, *J. Org. Chem.,* 2012, **77**, 8879-8887.

7 V. Percec, M. R. Imam, M. Peterca and P. Leowanawat, *J. Am. Chem. Soc.,* 2012, **134**, 4408-4420.

8 W. -R. Chen, L. Porcar, Y. Liu, P. D. Butler and L. J. Magid, *Macromolecules,* 2007, **40**, 5887-5898.

9 (a) P. Welch and M. Muthukumar, *Macromolecules,* 1998, **31**, 5892-5897; (b) E. N. Govorun, K. B. Zeldovich and A. R. Khokhlov, *Macromol. Theory Simul.,* 2003, **12**, 705-713.

10 (a) A. W. Freeman, R. H. Vreekamp and J. M. J. Fréchet, *Polym. Mater. Sci. Eng,.* 1997, **77**, 138-139; (b) Y. Wang, F. Zeng and S. C. Zimmernan, *Tetrahedron Lett.,* 1997, **38**, 5459-5462.

11 (a) M. Kawa and J. M. J. Fréchet, *Chem. Mater.,* 1998, **10**, 286-296; (b) M. Kawa and J. M. J. Fréchet, *Thin Solid Films,* 1998, **331**, 259-163.

12 P. -J. Yang, C. -W. Wu, D. Sahu and H. -C. Lin, *Macromolecules,* 2008, **41**, 9692-9703.

13 E. Lee, Y. -H. Jeong, J. -K. Kim and M. Lee, *Macromolecules,* 2007, **40**, 8355-8360.

14 (a) I. Gitsov and J. M. J. Fréchet, *J. Am. Chem. Soc.,* 1996, **118**, 3785-3786; (b) D. Yu, N. Vladimirov and J. M. J. Fréchet, *Macromolecules,* 1999, **32**, 5186-5192; (c) I. Gitsov, A. Simonyan, N. G. Vladimirov, *J. Polym. Sci. Part A: Polym. Chem.,* 2007, **45,** 5136-5148.

15 (a) I. T. Horváth and J. Rabai, *Science,* 1994, **266**, 72-75; (b) J. A. Gladysz, D. P. Curran and I. T. Horvath, (Eds.) *Handbook of Fluorous Chemistry*; Wiley-VCH: Weinheim, 2006.

16 N. Muller and H. Simsohn, *J. Phys. Chem.,* 1971, **75**, 942-945.

17 P. Ekwall, H. Eikrem and L. Mandell, *Acta Chem. Scand.*, 1963, **17**, 111-122.

18 D. F. Evans, *Proc. Chem. Soc.,* 1958, 115-116.

19 N. Muller and R. H. Birkhahn, *J. Phys. Chem.,* 1967, **71**, 957-962.

20 Z. -X. Jiang and Yu, Y. B. *J. Org. Chem.* **2010**, *75*, 2044-2049.

21 M. Taraban, Y. Feng, B. Hammouda, L. L. Hyland and Y. B. Yu, *Chem. Mater.,* 2012, **24**, 2299-2310.

22 A. Guinier, *Ann Phys (Paris),* 1939, **12**, 161–236.

23 (a) T. Li, N. Shao, Y. Liu, J. Hu, Y. Wang, L. Zhang, H. Wang, D. Chen and Y. Cheng, *J. Phys. Chem. B,* 2014, **118**, 3074-3084; (b) S. Rosenfeldt, E. Karpuk, M. Lehmann, H. Meier, P. Lindner, L. Harnau and M. Ballauff, *ChemPhysChem*., 2006, **7**, 2097-2104; (c) T. J. Prosa, B. J. Bauer and E. J. Amis, *Macromolecules,* 2001, **34**, 4897-4906.

24 M. Kotlarchyk and S. -H. Chen, *J. Chem. Phys.,* 1983, **79**, 2461-2469.

25 J. Ilavsky and P. Jemian, *J. Appl. Crystallogr.,* 2009, **42**, 347-353.

26 S. R. Kline, *J. Appl. Chrystallogr.,* 2006, **39**, 895-900.

27 (a) F. Michaux, J. -L. Blin, J. Teixeira and M. J. Stébé, *J. Phys. Chem. B,* 2012, **116**, 261-268; (b) R. H. Ottewill, A. R. Rennie and G. D. W. Johnson, *Adv. Colloid Interface Sci.,* 2003, **100-102**, 585-611; (c) M. Almgren, V. M. Garamus, L. Nordstierna, J. -L. Blin and M. J. Stébé, *Langmuir,* 2010, **26**, 5355-5363.

28 (a) G. Mathis, P. Leempoel, J. -C. Ravey, C. Selve and J. -J. Delpuech, *J. Am. Chem. Soc.,* 1984, **106**, 6162-6171; (b) M. Schmidt, D. Neger and W. Burchard, *Polymer*, 1979, **29**, 582-588.

29 (a) R. J. Ellis, *Curr. Opin. Struct. Biol.*, 2001, **11**, 114-119; (b) N. Tokuriki, M. Kinjo, S. Negi, M. Hoshino, Y. Goto, I Urabe and T. Yomo, *Prot. Sci.*, 2004, **13**, 125-133; (c) H. -X. Zhou, *FEBS Lett*., 2013, **587**, 1053-1061.

30 B. M. Tanda, N. J. Wagner, M. E. Mackay, C. J. Hawker and M. Jeong, *Macromolecules,* 2001, **34**, 8580-8585.

31 M.Trollsos, B. Atthof, A. Wirsch, J. L. Hedrick, J. A. Pople and A. P. Gast, *Macromolecules* **2000**, *33*, 6423-6438.

32 H. Vink, *J. Chem. Soc., Faraday Trans. 1,* 1985, **81**, 1725-1730.

33 J. Appell, G. Porte and E. Buhler, *J. Phys. Chem. B,* 2005, **109**, 13186-13194.

34 P. J. Daivis, D. N. Pinder and P. T. Callaghan, *Macromolecules,* 1992, **25**, 170-178.

35 S. J. Law and M. M. Britton, *Langmuir,* 2012, **28**, 11699-11706.

36 J. C. Sloop, *Rep. Org. Chem.,* 2013, **3**, 1-11.

37 D. H. Wu, A. D. Chen and C. S. Johnson, *J. Magn. Reson. A,* 1995, **115**, 260-264.

38 C. J. Glinka, J. G. Barker, B. Hammouda, S. Krueger, J. J. Moyer and W. J. Orts, *J. Appl. Crystallogr.*, 1998, **31**, 430-445.

39 D. I. Svergun, *J. Appl. Cryst.*, 1992, **25**, 495-503.

40 P. V. Konarev, V. V. Volkov, A. V. Sokolova, M. H. J. Koch and D. I. Svergun, *J Appl Cryst.*, 2003, **36**, 1277-1282.

41 D. Subramanian, D. A. Ivanov, I. K. Yudin, M. A. Anisimov and J. V. Sengers, *J. Chem. Eng. Data,* 2011, **56**, 1238−1248.